Eurographics Symposium on Rendering (2022)
A. Ghosh and L.-Y. Wei (Editors)

GAN-based Defect Image Generation for Imbalanced Defect Classification of OLED panels

Yongmoon Jeon[1] and Haneol Kim[1] and Hyeona Lee[1] and Seonghoon Jo[1] and Jaewon Kim[1]

[1]AI Team, Mechatronics Technology Center, Samsung Display Company, Korea

Abstract

Image classification based on neural networks has been widely explored in machine learning and most research have focused on developing more efficient and accurate network models for given image dataset mostly over natural scene. However, industrial image data have different features with natural scene images in shape of target objects, background patterns, and color. Additionally, data imbalance is one of the most challenging problems to degrade classification accuracy for industrial images. This paper proposes a novel GAN-based image generation method to improve classification accuracy for defect images of OLED panels. We validate our method can synthetically generate defect images of OLED panels and classification accuracy can be improved by training minor classes with the generated defect images.

CCS Concepts

• ***Applied computing*** → ***Computer-aided design;***

1. Introduction

Image classification is one of the most active research areas in machine learning. Deep learning (DL)-based classification techniques have been widely explored since AlexNet [KSH17] won ImageNet Large Scale Visual Recognition Challenge (ILSVRC) [RDSK15]. It achieved the lowest error rate of 15.3% with ImageNet dataset which was 10.8% lower than previous classification algorithms. Since then, more advanced DL approaches have been introduced and among them ResNet [HZRS16] accomplished 3.6% error rate which outperformed human experts with 5% error in average. Although such advanced DL networks can achieve good performance with ideal datasets such as MNIST, CIFAR, and IMAGENET [LBBH98, Kri09, DDSL09], they show low accuracy for unbalanced dataset where minor classes have smaller data size compared to other classes. Generally, unbalanced dataset suffer from overfitting problem incorrectly classifying minor classes as major classes with larger number of data. This paper proposes a novel image generation method, Defect Transfer GAN (DTGAN), to improve classification accuracy for unbalanced dataset by increasing the data size of minor classes. Our method synthetically generates defect images based on Generative Adversarial Network (GAN) [GPAMX14]. Conventional GANs could be applied for image generation of minor defects but their contribution for classification accuracy was limited since features of generated defects cannot faithfully reflect actual feature distribution due to training with insufficient dataset [RV19]. To overcome this limitation of conventional GANs, our method generates defect images by transferring actual defect features from large dataset into target images of minor classes as shown in Fig. 1. Let's assume we have sufficient defect images for Product A and we want to improve classification accuracy for Product B. We have sufficient defect-free images for Product B which is common situation in manufacturing since yield rate is generally much higher than failure rate. Our goal is generating defect images for Product B using its defect-free images reflecting feature distribution of defects in Product A. For this task, we propose DTGAN using paired dataset consisting of defect and defect-free images.

2. Related works

Image-to-image translation methods based on GAN can be classified as two categories: paired and unpaired dataset. GANs with paired dataset are trained by pairs of input and output images while the other category of GANs are trained by unpaired dataset. Generally, both categories of GANs can be applied for synthetic image generation and style conversion but the former category with paired dataset is known to be advantageous for specifying outputs.

2.1. Image to image translation with paired dataset

Pix2pix exploited Conditional GAN as a unified platform for various applications such as image generation with semantic label, object generation from an edge map, and colorization from a grayscale image [IZZE17]. Pathak et al. demonstrated adding a conventional loss like L1 or L2 distance to GAN loss function can be effective for similar image generation with a target image [PKDD16]. Our problem is generating a defect image of an

© 2022 The Author(s)
Eurographics Proceedings © 2022 The Eurographics Association.

DOI: 10.2312/sr.20221164

delivered by EUROGRAPHICS DIGITAL LIBRARY www.eg.org diglib.eg.org

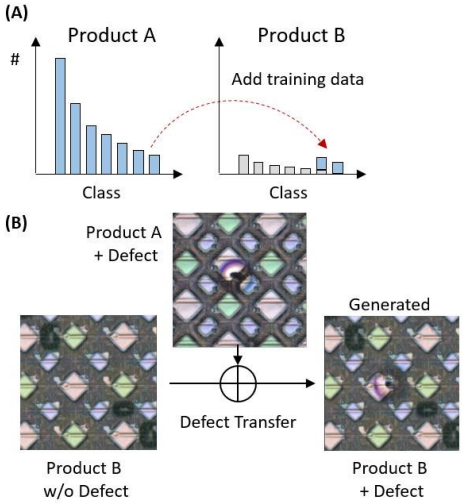

Figure 1: *Transferring defect features from Product A to Product B for balancing dataset of each class. (A) Sufficient dataset for Product A can be utilized to balance dataset for Product B. (B) For defect classification, insufficient image of minor classes for Product B can be augmented by synthetically generating defect images using feature transferring from sufficient dataset for Product A.*

OLED panel from a defect-free image while preserving a complex electronic circuit pattern so we adopted L1 distance in our loss function. Isola et al. showed L1 distance produced less blur effect than L2 distance [IZZE17]. They required paired dataset to compute L1 loss which additionally made the network converging faster than typical GANs. Despite its good performance, applications were limited due to impracticalness of obtaining paired dataset. We overcome such limitation by introducing an acquisition method of paired dataset with Inpaint net based on Contextual Attention GAN [YLYS18].

2.2. Image to image translation with unpaired dataset

Many neural networks with unpaired dataset have been presented for synthetic image generation through feature transferring scheme such as CycleGAN [ZPI*17], StyleGAN [KLA19], and StarGAN [CCKH18,CUYH20]. While transferring and preserving features can be explicitly trained by paired dataset, establishing paired dataset with the same feature relationship is a challenging task. Methods with unpaired dataset are advantageous with easy establishment of database but require additional tricks to control transferring features. CycleGAN proposed a consistency loss function proportional to the difference between input and generated images to keep the originality of the input image. StyleGAN could train only the style of source images by Adaptive Instance Normalization [HB17]. While StyleGAN-based approaches required separate training for specific style transfer from unpaired dataset, StarGAN allowed to train various styles from single dataset in multiple feature domain. Generally, those generative networks were designed for natural scene images where high-level features like hairstyle, makeup, age, and glasses were assumed as transferring styles and

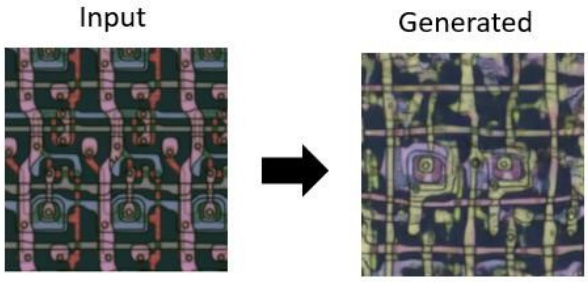

Figure 2: *Limitation of a conventional GAN. Originality of an input image, electronic circuit pattern of an OLED panel, cannot be preserved in a generated image by a conventional GAN, StarGAN-v2.*

low-level features like pose, gesture, and shape were as originality of the input. Unlike such a natural scene image, our target is electronic circuit images obtained from OLED manufacturing processes where definition of styles is not valid. Therefore, we exploited a mask image to explicitly define transferring and preserving features in paired dataset.

2.3. GAN-based Image Inpainting

Inpaining methods based on neural networks have been widely applied to various computer vision tasks including photo editing, image-based rendering, and VR/AR. A technical challenge is generating seamless and visually consistent pixels with neighboring pixels in ROI (Region Of Interest) without any boundary artifacts and blurry texture

3. Defect Transfer GAN (DTGAN)

Many neural networks have been introduced for synthetic image generation by feature transferring such as Pix2Pix

3.1. Architecture of DTGAN

Generally it is impossible to acquire both defect and non-defect image pair for the same region of an OLED panel. So we applied Inpaint based on Contextual Attention GAN [YLYS18] to replace a defect region in a defect image with a normal region as shown in Fig. 3 (A). This is a key step of our method to overcome the impracticalness of generative networks with paired dataset despite their good performance. This process also benefits from easy access to huge amount of defect-free images since stable OLED manufacturing process generally achieves over 90% yield rate which means the rate of defective and non-defective panels is 1:9. Then, we train an adversarial network with the paired dataset of defect and defect-free images. We used the paired dataset and a mask image as input for our generative network. The mask image as shown in Fig. 3 (B) is a binary image where white and black pixels correspond to defect and defect-free regions, respectively. We exploited a mask image to explicitly specify region to be defect. The mask image allows a generator in Fig. 3 (B) to focus on the defect region. We added the

© 2022 The Author(s)
Eurographics Proceedings © 2022 The Eurographics Association.

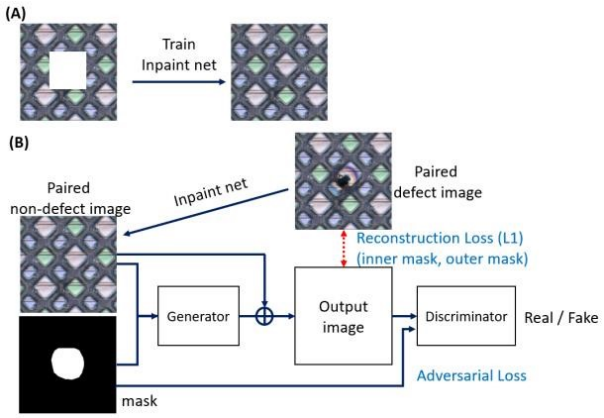

Figure 3: *Architecture of DTGAN. It consists of Inpaint net to generate a defect-free image from a defect image and GAN to train relationship between a pair of defect and defect-free images. The defect region in the defect image is specified by a mask image.*

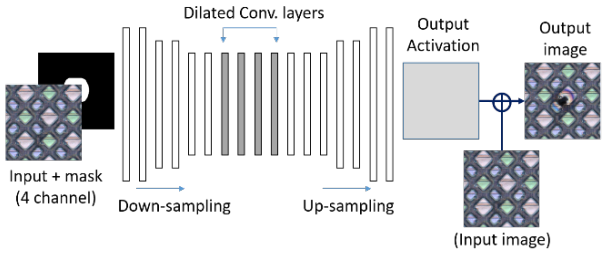

Figure 4: *Architecture of generator in DTGAN. It consists of 17 convolutional layers with 2 down-sampling, 2 up-sampling, and 4 dilated layers being inputted by a defect-free and a mask image.*

defect-free image to activation of the generator to keep the background pattern of the defect-free image. A discriminator judges the output of generator as a real or fake image and the overall network is trained to minimize a loss function.

3.2. Generator

Our generator is inputted by a four channel image which consists of a defect-free image (RGB 3 channel) and a mask image (Binary 1 channel) in Fig. 4. We designed the generator with 17 convolutional layers including 2 down-sampling, 2 up-sampling, and 4 dilated convolutional layers. To generate a sharp image in high-resolution, we minimized down-sampling layers and added more dilated convolutional layers to increase a receptive field. We used ReLU as an activation function and spectral normalization (SN) since batch normalization tends to distort a region with a mono-color pattern.

3.3. Discriminator

Our discriminator consists of two discriminators to enhance the texture quality of an output image: global and local discriminators which cover 256×256 and 64×64 pixel regions, respectively. Input was a 4 channel image with defect and mask images. The global discriminator was trained to judge the defect image between real or fake images through 6 convolutional layers. The local discriminator was trained for the same job based on detail features and texture in a local region through 4 convolutional layers sharing weights. Outputs of global and local discriminators were concatenated into a fully connected layer to make a final judgement where WGAN (Wasserstein GAN) was used to maximize training stability [ACB17].

3.4. Objective Function

Our generator and discriminators were trained with following loss function in (1) where G and D indicate generator and discriminator, respectively. The novelty of our objective function is the separate weights for defect and background (defect-free) regions. In the equation, 'inner' and 'outer' means two regions for generating defect and background texture, respectively. The two regions are defined by the white and black pixels in the mask image corresponding to 'inner' and 'outer' regions. We used a greater value for the C_2 than C_1 ($C_2 > C_1$) to preserve the texture of defect-free region in an input image and increase the generative effect of defect.

$$Loss = arg\ min_G min_D\ C_{GAN}L_{GAN}(G,D) + C_1 L_{1,inner}(G) + C_2 L_{1,outer}(G) \quad (1)$$

3.5. Training Procedure

This section describes a pipeline for our training method. First, it starts with training Inpaint GAN [YLYS18] using 500 defect-free images. The images were randomly blocked by a square and the network generated a texture image for the blocked region while being trained for minimizing difference between the generated region and the mask region of the original image. Secondly, we created mask images in Fig. 3 for 100-200 defect images. Then, box mask images were created from the mask image in the condition that a rectangle included a defect region of the mask image as shown in the first row of Fig. 6. By inputting a box mask image and a defect image into the trained Inpaint GAN, it converted the defect region to a defect-free region as shown in the third row of Fig. 6. It is crucial for the defect generation quality of DTGAN to use a box mask image instead of a mask image for Inpaint GAN. Slight seams around the edge of mask in the generated defect-free image cannot be unavoidable and they can be trained as defect region by DTGAN if it uses the same box mask image. That is, by using different mask images for Inpaint GAN and DTGAN, generative errors near the edge of mask can be avoidable. Lastly, we trained DTGAN using a generated defect-free image, an original defect image, and a mask image. To optimize training with a limited number of images, we made random augmentation at each epoch such as resized crop, rotate, flip, CLAHE, brightness, and contrast using python albumentation package [BIKP20]. The later 3 augmentation methods were not applied to mask images.

© 2022 The Author(s)
Eurographics Proceedings © 2022 The Eurographics Association.

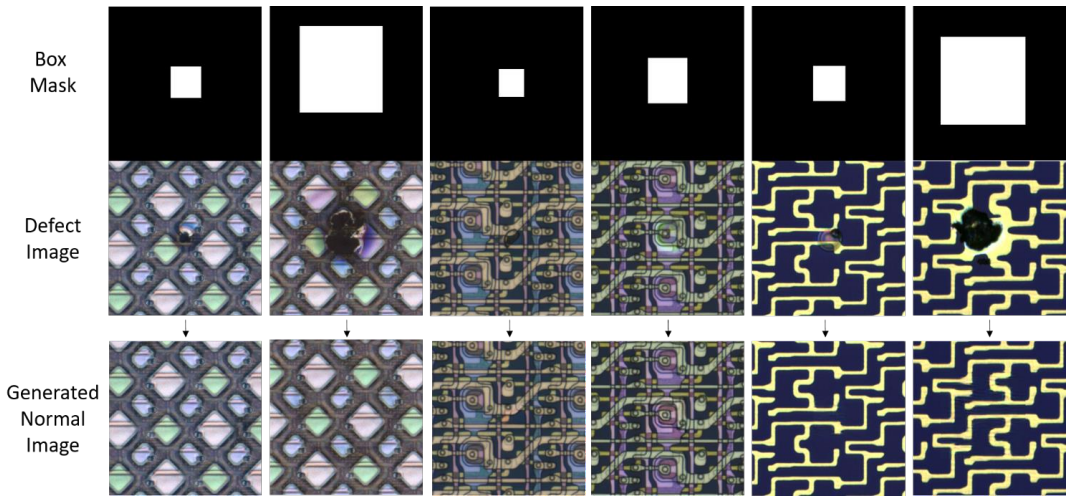

Figure 6: *Inpaint GAN results for defect images of OLED panels in different manufacturing processes. It generates a defectfree images from a defect image and the defect position is specified by a box mask image which is manually created.*

3.6. Defect Image Generation

We generated a defect region in a defect-free image using the trained DTGAN. The input of DTGAN was a defect-free image and a mask image to set position, size, and boundary shape of a defect. We could generate various defect images from the same defect-free image using different mask images as shown in Fig. 7. We applied the same mask used for training and newly generated masks for varying the size and location of defects.

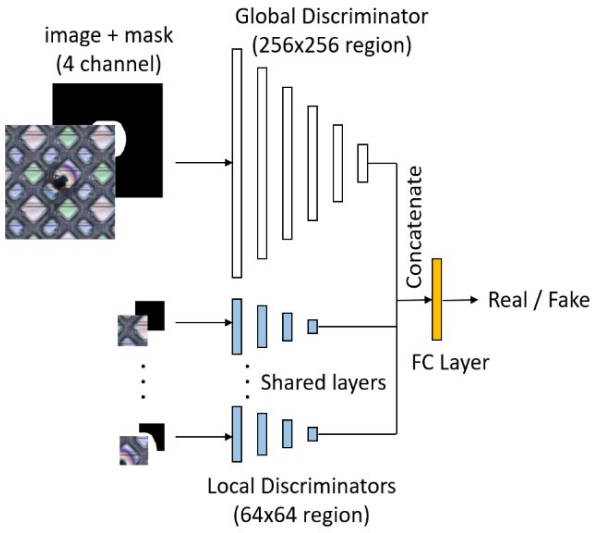

Figure 5: *Architecture of discriminator in DTGAN. It consists of global and local discriminators which covers 256×256 and 64×64 pixel region, respectively. The global region in 256×256 pixels is divided into 4×4 grid patches. These patches are fed into 16 local discriminators which share weight parameters.*

4. Results

4.1. Inpaint GAN

We tested the performance of Inpaint GAN using various inspection images acquired from OLED manufacturing processes as shown in Fig. 6. The input of Inpaint GAN is a box mask image and a defect image in the first and the second row. A defect-free image in the third row was generated from the defect image by replacing the defect region with a normal region. Note that the defect images with complicated patterns were successfully changed to defect-free images without any visible flaws and seams by the Inpaint GAN. We trained Inpaint GAN separately for images with the same pattern, obtained from the same manufacturing process, to improve the generation quality of defect-free images. In the Fig. 6, 1-2, 3-4, and 5-6 columns were grouped together for training Inpaint GAN separately. The performance of Inpaint GAN depends on the size of defect region. It failed in the case that the size of defect region was similar with the entire image. Empirically, we found it achieved good performance when defect region was smaller than one over third of the image.

4.2. DTGAN

We tested the defect generation of DTGAN with images with various patterns as shown in Fig. 7. For the best generation quality, we trained it with the same type of pattern and defect shape, a black spot in a colorful circle, in Fig. 7 (A). The results in Fig. 7 (B) were generated by the trained DTGAN from defect-free images with a familiar background circuit pattern (seen during training). The generation results reflect faithfully the characteristic of real defects making hard to distinguish between real and generated defect images. The color of a circle in the defect region varies depending on the background color and such feature is reflected in the defect region of generated images. The size, position and boundary of defect region can be controlled by an input mask image. We evaluated the generation performance of DTGAN with unseen

© 2022 The Author(s)
Eurographics Proceedings © 2022 The Eurographics Association.

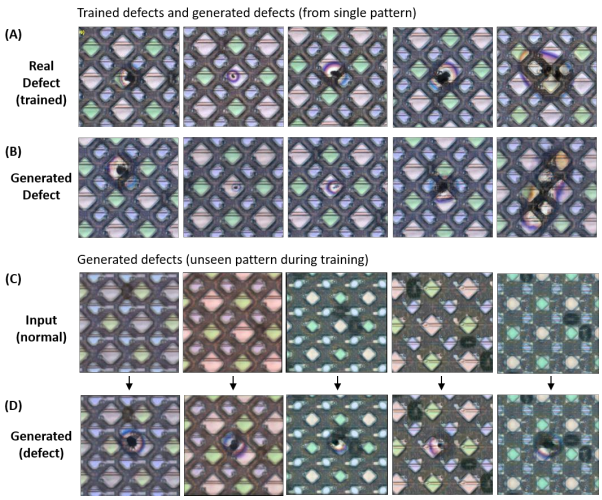

Figure 7: *Generated defect images. Our DTGAN generates synthetic defect images, (B) and (D), in high quality which are almost impossible to distinguish from real defect images in (A). Results in (B) were generated from defectfree image of trained pattern. Results in (D) were generated from defect-free images in (C) which patterns were not seen during training.*

background circuit pattern images in Fig. 7 (C) which were not included in the training dataset. The results in Fig. 7 (D) validate our DTGAN can faithfully generate defect images from untrained defect-free images. Fig. 8 shows generation results using defect-free images with two different types of patterns and five different defect shapes as shown in (A). The results with trained and untrained background pattern are shown in Fig. 8 (B) and (C), respectively. For these multiple types of defects generation, we trained separate networks each. Note that DTGAN can generate defect images in not only overlapping manner with a background pattern, 1-3 columns, but also erasing or transforming manner of a background pattern, 4-5 columns.

4.3. Classification accuracy with generated defect images

We validated that defect classification accuracy can be improved with defect images generated by DTGAN. First, we trained DTGAN for Defect A class with 150 images in the first row pattern of Fig. 8. Then, we generated synthetic Defect A images for new pattern in the third row of Fig. 8. Finally, we evaluated classification accuracy with 20 defect classes including Defect A for four cases as following: (a) without any real and fake images for Defect A (b) with 200 real images for Defect A (c) with 4000 fake images for Defect A (d) with 200 real and 4000 fake images for Defect A

The total training and test dataset for 19 classes except Defect A is 76k and 19k, respectively. Fig. 9 shows recall values of classification for the four cases. 0.1 recall score in case (b) was increased to 0.65 with case (c) where only fake defect images were used for training in much greater number. We could achieve slightly improved recall score by small increase of training dataset with real defect images in case (d). Significant increase of recall score between case (b) and (c) verifies that defect generation quality of DTGAN is comparable to real defect images and the generated defect images can contribute to improve defect classification accuracy for minor classes with small number of training images. The precision scores are 0, 0.97, 0.73, 0.84 for four cases, respectively.

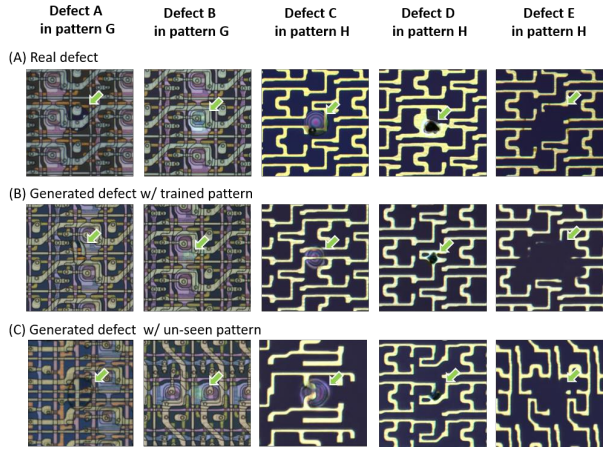

Figure 8: *Generated defect images for five defect types, Defect A E, in two different manufacturing processes marked as pattern G and H. (B) and (C) show results from trained and untrained pattern images, respectively. Green arrows indicate defect regions.*

5. Conclusions

This paper proposes a novel DTGAN method to generate a synthetic image using paired dataset consisting of feature-existing and feature-free images. Such generated images can be used to improve classification accuracy for imbalanced dataset where minor classes with insufficient data could cause overfitting problem. We applied this method to improve defect classification accuracy of

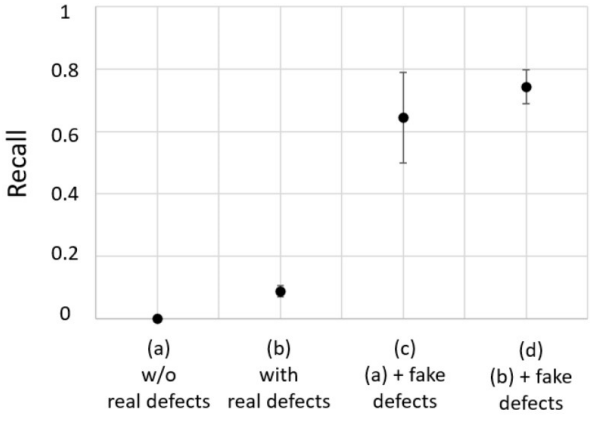

Figure 9: *Improved recall value of a classifier which was trained by the generated defect images. Dots and bars indicate average and standard deviation of recall values for five trained classifiers.*

© 2022 The Author(s)
Eurographics Proceedings © 2022 The Eurographics Association.

OLED inspection process commonly suffering from imbalanced defect database. We expect our method can be utilized in various applications where only specific feature information is required to transfer to another image while keeping other regions unchanged.

References

[ACB17] ARJOVSKY M., CHINTALA S., BOTTOU L.: Wasserstein generative adversarial networks. *Proceedings of the 34th International Conference on Machine Learning* (2017). 3

[BIKP20] BUSLAEV A., IGLOVIKOV V., KHVEDCHENYA E., PARINOV A. E. A.: Albumentations: Fast and flexible image augmentations. *MDPI* (2020). 3

[CCKH18] CHOI Y., CHOI M., KIM M., HA J. E. A.: Stargan:unified generative adversarial networks for multi-domain image-to-image translation. *CVPR* (2018). 2

[CUYH20] CHOI Y., UH Y., YOO J., HA J.: Stargan v2: Diverse image synthesis for multiple domains. *CVPR* (2020). 2

[DDSL09] DENG J., DONG W., SOCHER R., LI L. E. A.: Imagenet: A large-scale hierarchical image database. *CVPR* (2009). 1

[GPAMX14] GOODFELLOW I., POUGET-ABADIE J., MIRZA M., XU B.: Generative adversarial networks. *NIPS* (2014). 1

[HB17] HUANG X., BELONGIE S.: Arbitrary style transfer in realtime with adaptive instance normalization. *ICCV* (2017). 2

[HZRS16] HE K., ZHANG X., REN S., SUN J.: Deep residual learning for image recognition. *CVPR* (2016). 1

[IZZE17] ISOLA P., ZHU K., ZHOU T., EFROS A.: Image-to-image translation with conditional adversarial networks. *CVPR* (2017). 1, 2

[KLA19] KARRAS T., LAINE S., AILA T.: A style-based generator architecture for generative adversarial networks. *CVPR* (2019). 2

[Kri09] KRIZHEVSKY A.: Learning multiple layers of features from tiny images. *MasterâĂŹs thesis, Department of Computer Science, University of Toronto* (2009). 1

[KSH17] KRIZHEVSKY A., SUTSKEVER I., HINTON G.: Imagenet classification with deep convolutional neural networks. *Communications of the ACM* (2017). 1

[LBBH98] LECUN Y., BOTTOU L., BENGIO Y., HAFFNER P.: Gradient-based learning applied to document recognition. *Proceedings of the IEEE* (1998). 1

[PKDD16] PATHAK D., KRAHENBUHL P., DONAHUE J., DARRELL Y. E. A.: Context encoders: Feature learning by inpainting. *CVPR* (2016). 1

[RDSK15] RUSSAKOVSKY O., DENG J., SU H., KRAUSE J. E. A.: Imagenet large scale visual recognition challenge. *IJCV* (2015). 1

[RV19] RAVURI S., VINYALS O.: Seeing is not necessarily believing: Limitations of biggans for data augmentation. *ICLR* (2019). 1

[YLYS18] YU J., LIN Z., YANG J., SHEN X. E. A.: Generative image inpainting with contextual attention. *CVPR* (2018). 2, 3

[ZPI*17] ZHU J., PARK T., ISOLA P., EFROS A., ZHU J. E. A.: Unpaired image-to-image translation using cycle-consistent adversarial networks. *ICCV* (2017). 2

© 2022 The Author(s)
Eurographics Proceedings © 2022 The Eurographics Association.